



# Asteroid impact, not volcanism, caused the end-Cretaceous dinosaur extinction

Alfio Alessandro Chiarenza<sup>a,b,1,2</sup> , Alexander Farnsworth<sup>c,1</sup> , Philip D. Mannion<sup>b</sup> , Daniel J. Lunt<sup>c</sup> , Paul J. Valdes<sup>c</sup>, Joanna V. Morgan<sup>a</sup>, and Peter A. Allison<sup>a</sup>

<sup>a</sup>Department of Earth Science and Engineering, Imperial College London, South Kensington, SW7 2AZ London, United Kingdom; <sup>b</sup>Department of Earth Sciences, University College London, WC1E 6BT London, United Kingdom; and <sup>c</sup>School of Geographical Sciences, University of Bristol, BS8 1TH Bristol, United Kingdom

Edited by Nils Chr. Stenseth, University of Oslo, Oslo, Norway, and approved May 21, 2020 (received for review April 1, 2020)

**The Cretaceous/Paleogene mass extinction, 66 Ma, included the demise of non-avian dinosaurs. Intense debate has focused on the relative roles of Deccan volcanism and the Chicxulub asteroid impact as kill mechanisms for this event. Here, we combine fossil-occurrence data with paleoclimate and habitat suitability models to evaluate dinosaur habitability in the wake of various asteroid impact and Deccan volcanism scenarios. Asteroid impact models generate a prolonged cold winter that suppresses potential global dinosaur habitats. Conversely, long-term forcing from Deccan volcanism (carbon dioxide [CO<sub>2</sub>]-induced warming) leads to increased habitat suitability. Short-term (aerosol cooling) volcanism still allows equatorial habitability. These results support the asteroid impact as the main driver of the non-avian dinosaur extinction. By contrast, induced warming from volcanism mitigated the most extreme effects of asteroid impact, potentially reducing the extinction severity.**

Dinosauria | extinction | end-Cretaceous | Chicxulub | Deccan

The end-Cretaceous mass extinction, 66 Ma, is the most recent of Raup and Sepkoski's (1) "Big Five" extinction events (2). Non-avian dinosaurs, along with many other groups that had dominated the Earth for 150 My, went extinct. Although there is still debate as to whether dinosaurs were already in decline (3) prior to their extinction, their fossil record demonstrates global survival until the terminal Cretaceous and unambiguous absence thereafter. The Cretaceous/Paleogene (K/Pg) mass extinction coincided with two major global environmental perturbations: heightened volcanism associated with the Deccan Traps and the Chicxulub asteroid impact (Fig. 1A) (4). The relative roles of these two potential kill mechanisms on the timing and magnitude of the extinction have been fiercely debated for decades (4, 5). The Maastrichtian has been shown to have a relatively high climate sensitivity (6), meaning even relatively small perturbations to the system could potentially have a catastrophic impact.

The Deccan Traps, in present-day west-central India (7), formed from a series of short (~100-ky) intermittent eruption pulses (8), with two main phases (8, 9) at ~67.4 Ma (toward the end of the Cretaceous) and ~66.1 Ma (starting just before the boundary and continuing through the earliest Paleogene) erupting an estimated >10<sup>6</sup> km<sup>3</sup> of magma over a duration of ~710,000 y (9, 10). This volcanism released radiatively active atmospheric gases, particularly carbon dioxide (CO<sub>2</sub>) and sulfur dioxide (SO<sub>2</sub>), which are thought to have promoted global climate change (11, 12). Most authors have argued for global average temperature excursions of ±2 °C in relation to these pulses (7, 8) (although see ref. 9 for a contrasting view on such correlations). Under this scenario, this potential kill mechanism either led directly to mass extinction (5) or sufficiently stressed global ecosystems that they became vulnerable to subsequent agents (13). Given that intense and prolonged volcanism appears to be the primary kill mechanism for earlier mass extinctions (14–16), it is considered by some as the most likely candidate to explain the K/Pg mass extinction

(17). However, the timing and size of each eruptive event are highly contentious in relation to the mass extinction event (8–10).

An asteroid, ~10 km in diameter, impacted at Chicxulub, in the present-day Gulf of Mexico, 66 Ma (4, 18, 19), leaving a crater ~180 to 200 km in diameter (Fig. 1A). This impactor struck carbonate and sulfate-rich sediments, leading to the ejection and global dispersal of large quantities of dust, ash, sulfur, and other aerosols into the atmosphere (4, 18–20). These atmospheric contaminants led to prolonged sunlight screening and global cooling (19–22), with severe ecological cascade effects (4, 13, 23). The impact is hypothesized to have precipitated an extremely cold "impact winter" that was beyond the thermophysiological limits of much of the end-Cretaceous biota (23). A globally ubiquitous ejecta layer (23) overlies the latest Cretaceous fossiliferous horizons, marking a biotic change after the K/Pg boundary (Fig. 1A). The size of this impact, its hypothesized global climatic effects, and the worldwide absence of non-avian dinosaurs after it

## Significance

**We present a quantitative test of end-Cretaceous extinction scenarios and how these would have affected dinosaur habitats. Combining climate and ecological modeling tools, we demonstrate a substantial detrimental effect on dinosaur habitats caused by an impact winter scenario triggered by the Chicxulub asteroid. We were not able to obtain such an extinction state with several modeling scenarios of Deccan volcanism. We further show that the concomitant prolonged eruption of the Deccan traps might have acted as an ameliorating agent, buffering the negative effects on climate and global ecosystems that the asteroid impact produced at the Cretaceous–Paleogene boundary.**

Author contributions: A.A.C., A.F., P.D.M., J.V.M., and P.A.A. designed research; A.A.C., A.F., and P.D.M. performed research; D.J.L. contributed new reagents/analytic tools; A.A.C., A.F., and P.J.V. analyzed data; D.J.L., P.J.V., and J.V.M. contributed to experimental design of the GCMs; A.A.C., A.F., and P.D.M. wrote the paper; and D.J.L., P.J.V., J.V.M., and P.A.A. contributed to writing the paper.

The authors declare no competing interest.

This article is a PNAS Direct Submission.

This open access article is distributed under [Creative Commons Attribution-NonCommercial-NoDerivatives License 4.0 \(CC BY-NC-ND\)](https://creativecommons.org/licenses/by-nc-nd/4.0/).

Data deposition: All datasets, model outputs, and R scripts are available on Figshare (Data S1, DOI: [10.6084/m9.figshare.11908179](https://doi.org/10.6084/m9.figshare.11908179); Data S2, DOI: [10.6084/m9.figshare.11908203](https://doi.org/10.6084/m9.figshare.11908203); Data S3, DOI: [10.6084/m9.figshare.11908227](https://doi.org/10.6084/m9.figshare.11908227); Data S4, DOI: [10.6084/m9.figshare.11908284](https://doi.org/10.6084/m9.figshare.11908284); Data S5, DOI: [10.6084/m9.figshare.11908266](https://doi.org/10.6084/m9.figshare.11908266); Data S6, DOI: [10.6084/m9.figshare.11908305](https://doi.org/10.6084/m9.figshare.11908305); Data S7, DOI: [10.6084/m9.figshare.11908311](https://doi.org/10.6084/m9.figshare.11908311); Data S8, DOI: [10.6084/m9.figshare.11908365](https://doi.org/10.6084/m9.figshare.11908365); Data S9, DOI: [10.6084/m9.figshare.11908368](https://doi.org/10.6084/m9.figshare.11908368); Data S10, DOI: [10.6084/m9.figshare.11908374](https://doi.org/10.6084/m9.figshare.11908374); Data S11, DOI: [10.6084/m9.figshare.11908407](https://doi.org/10.6084/m9.figshare.11908407); Data S12, DOI: [10.6084/m9.figshare.11908416](https://doi.org/10.6084/m9.figshare.11908416); Data S13, DOI: [10.6084/m9.figshare.11908422](https://doi.org/10.6084/m9.figshare.11908422); and Data S14, DOI: [10.6084/m9.figshare.11908437](https://doi.org/10.6084/m9.figshare.11908437)).

<sup>1</sup>A.A.C. and A.F. contributed equally to this work.

<sup>2</sup>To whom correspondence may be addressed. Email: [a.chiarenza15@gmail.com](mailto:a.chiarenza15@gmail.com).

This article contains supporting information online at <https://www.pnas.org/lookup/suppl/doi:10.1073/pnas.2006087117/-DCSupplemental>.

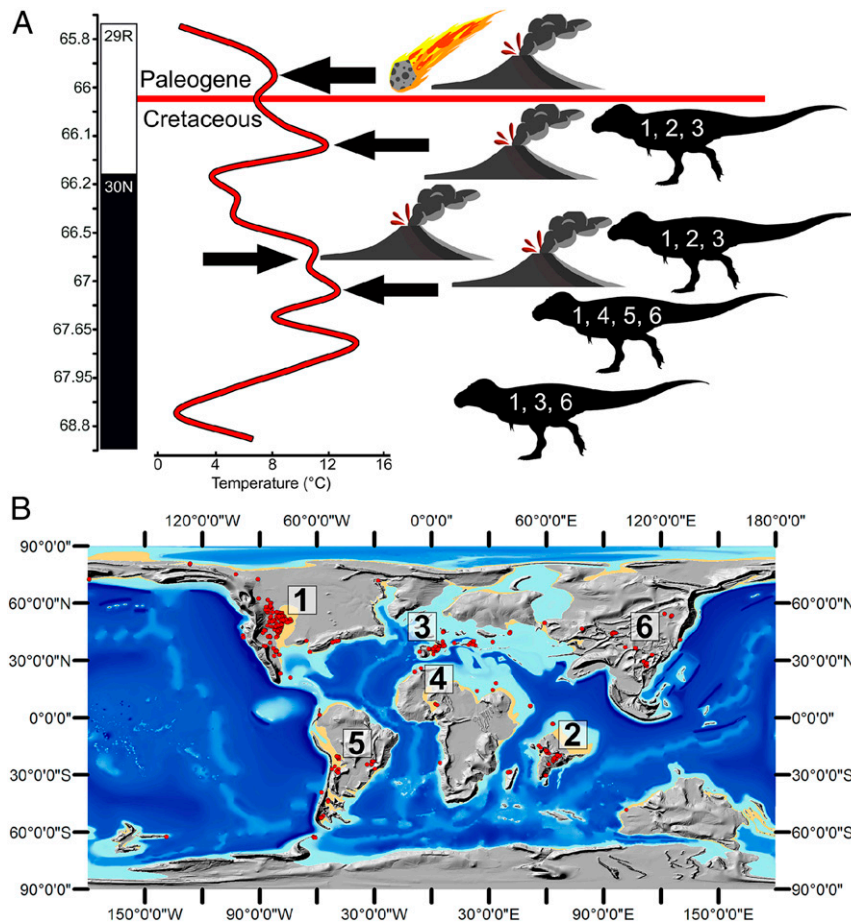


**Fig. 1.** Geologic (A) and paleontological (B) records of the K/Pg mass extinction. Paleothermometer (A) showing the Deccan-induced warming with the two main episodes of volcanism highlighted by the black arrows and symbols of volcanoes. The last phase extends beyond the end of the Cretaceous, characterized by the bolide impact in Chicxulub. Fossil remains of non-avian dinosaurs (body fossils, egg fragments, and nesting sites) occur throughout the whole stratigraphic record of prolonged volcanism episodes (dinosaur silhouettes). Numbers represent upper Maastrichtian dinosaur bearing localities, mapped on a late Maastrichtian paleogeography in B. 1, Hell Creek Formation (United States); 2, Lameta Formation (India); 3, Tremp Formation (Spain); 4, Phosphorite beds (Morocco); 5, Marília Formation (Brazil); 6, Nemegt Formation (Mongolia). Dinosaur silhouette image credit: Phylopic/Jack Mayer Wood, which is licensed under [CC BY 3.0](https://creativecommons.org/licenses/by/3.0/).

(Fig. 1B) suggest a direct causal relationship between these phenomena (4, 23).

Several modeling approaches have attempted to reproduce the climatic conditions at the K/Pg boundary (20–22), but none have so far quantified the abiotic effect on biological habitability. Herein, we model the climatic conditions at the end-Cretaceous, including the perturbations caused by the two potential extinction drivers. We use habitat suitability modeling to test the effect of these perturbations on the distribution of the dominant Cretaceous terrestrial group, the non-avian dinosaurs.

## Results

The climatic perturbations generated by Deccan volcanism [67.4 to 65.5 Ma (24)] and the asteroid impact [66.0 Ma (25)] are evaluated using coupled atmosphere–ocean general circulation model (AOGCM; forced by K/Pg boundary conditions) simulations (Fig. 2), which account for the combined effects of aerosol injection (ash, sulfate aerosol, and soot deposition affecting surface light reflectance) that cool the climate, with secondary effects such as changes in surface albedo (snow and sea-ice feedback), as well as atmospheric gasses ( $\text{CO}_2$ ) that warm the climate. Ozone concentrations are prescribed at modern-day values. The climate response is calculated using the mean of the last 50 y as well as the

3 y mean centered on the peak cooling event in the transient simulations. Climate simulations replicate the effect of volcanism, both short-term aerosol injection (tens of years) and long-term  $\text{CO}_2$  forcing (hundreds of years), and asteroid impact in isolation (decoupled, excluding long-term concurrent Deccan  $\text{CO}_2$  forcing, experiments) (*SI Appendix, Figs. S1 and S2*) and together (coupled, inclusive of Deccan  $\text{CO}_2$  forcing, experiments) (*SI Appendix, Figs. S3–S6*) by means of transient aerosol forcing, where all climatic perturbations evolved with time (*SI Appendix, Fig. S7*). Sensitivity experiments that varied the magnitude of the different perturbations were used to account for variations in the severity of these extreme events (*SI Appendix, Table S1*).

In the decoupled experiments (Table 1 and *SI Appendix, Table S1*), a 5 to 15% solar dimming reduction is considered to simulate the effects of Deccan volcanism or asteroid-induced cooling through reduction in incident shortwave radiation ( $-67.9$  to  $-203.6 \text{ W/m}^2$ ), within the predicted range of Kaiho et al. (18). However, the higher-end estimate is considered too extreme by some regarding Deccan volcanism, with Schmidt et al. (16) suggesting that the reduction in global mean surface temperature from a Deccan magnitude eruption represents no more than a  $-4.5 \text{ }^\circ\text{C}$  reduction in surface cooling. This is less than the predicted cooling from the 5% scenario ( $-9.7 \text{ }^\circ\text{C}$ ), suggesting that

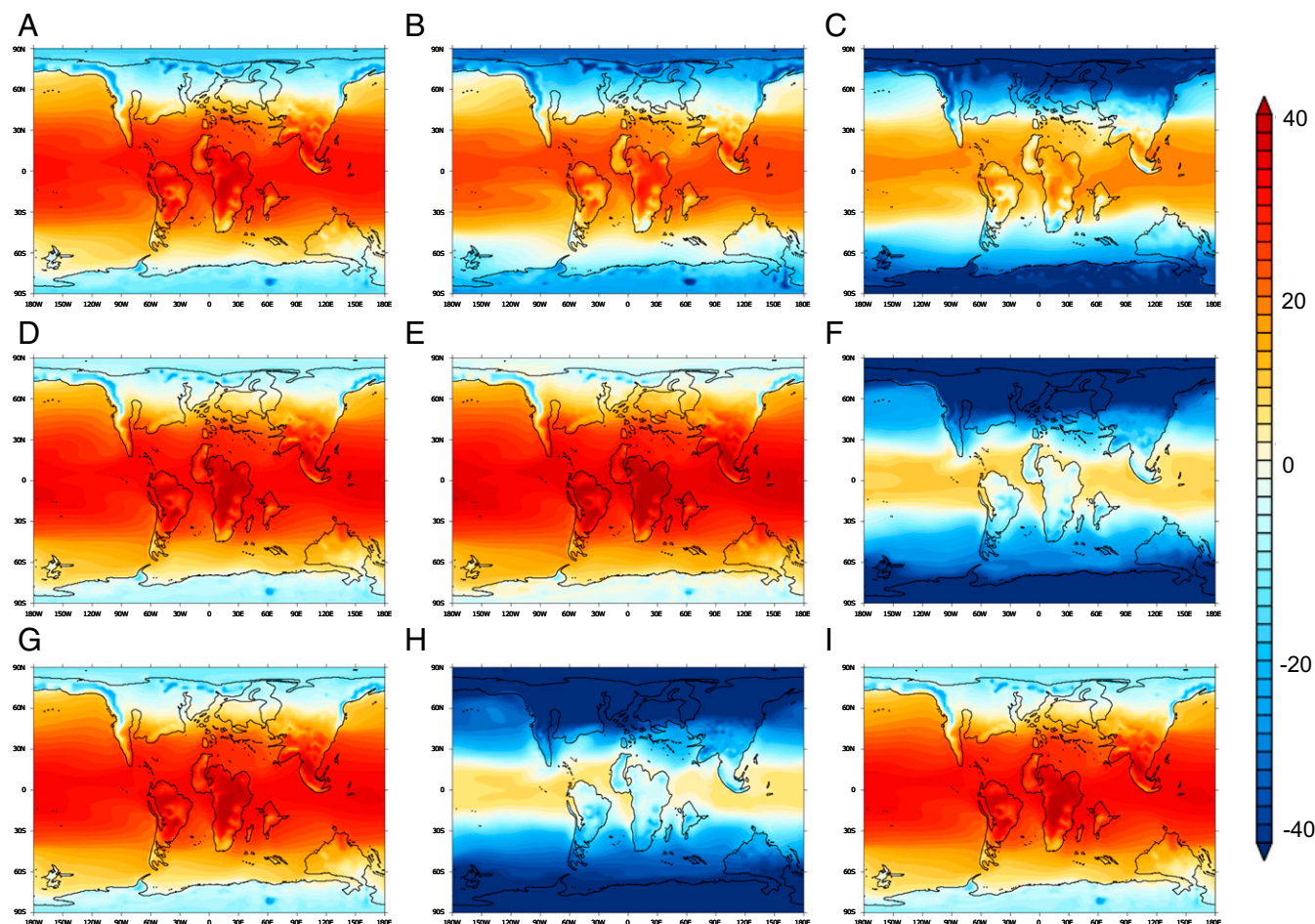


**Fig. 2.** K/Pg surface temperature (degrees Celsius) outputs from GCMs. Heat maps represent temperature fluctuations from the late Maastrichtian control, with cooler temperatures in blue and warmer temperatures in red. Late Maastrichtian climate control (A) is perturbed in B by a solar dimming simulation reproducing the effect of mild asteroid impact or extreme volcanism-induced cooling (B) at 5% (scenario 1) and of a more extreme asteroid-induced cooling scenario (C) at 10% (scenario 2) of solar radiation reduction. The effect of prolonged volcanism is reproduced with an increase to 1,120 ppm of (D) CO<sub>2</sub> content (scenario 5) and to (E) 1,680 ppm of CO<sub>2</sub> (scenario 6). A transient model including both Deccan volcanism and the effect of the Chicxulub impact is shown in F (scenario 11) and G (scenario 12), and with inactive volcanism (H, scenario 13 and I, scenario 14), while the three coldest years of the impact are modeled in F (scenario 11) and H (scenario 13) (additional details and figures on GCMs are in *SI Appendix*). Temperature scale runs from  $-40^{\circ}\text{C}$  to  $40^{\circ}\text{C}$ .

atmospheric cooling as a result of Deccan volcanism will not drive swings in temperature and precipitation that would lead to an extinction-level event.

These scenarios only represent a reduction in solar luminosity (in the case of  $-5\%$  volcanism-induced solar dimming, this assumes the best-case scenario [smallest climate forcing] whereby constant volcanic eruption allows replenishment of stratospheric aerosols at the same rate as aerosol loss from the stratosphere) without CO<sub>2</sub> release during  $10^2$  y of run time. As such, these solar dimming experiments give Deccan volcanism the best possible chance of inflicting an abiotic extinction-level event through assuming long-term (1,000 y) cooling (decreased solar forcing, mimicking constant aerosol loading of the stratosphere) that is yet to be proven in the rock record (16). Further simulations, with solar luminosity reduced by 10, 15, and 20% of the end-Cretaceous “norm,” evaluated progressively more extreme asteroid impact scenarios, which have been previously considered to be equivalent (18, 25) to a 10 to 20% lowering of solar input. Two additional simulations assessed the long-term ( $10^3$  y) warming effect caused by Deccan volcanism resulting from increased atmospheric CO<sub>2</sub> release. Both represent extreme scenarios supported by long-term proxy evidence of an increase in atmospheric

CO<sub>2</sub> from the 560-ppm baseline in the experiment to 1) 1,120 ppm (26) and 2) 1,680 ppm (27, 28).

The simulations show that solar dimming (Table 2 and *SI Appendix*, Table S2) would have generated global cooling of between  $9.7^{\circ}\text{C}$  and  $66.8^{\circ}\text{C}$  (in the most extreme scenario [20% solar dimming]) (Fig. 2 B and C and Table 2) on land but that the addition of CO<sub>2</sub> from Deccan volcanism offset this cooling by warming of  $+4.7^{\circ}\text{C}$  to  $+8.75^{\circ}\text{C}$  (Fig. 2 D and E and Table 2). Multiproxy reconstructions from Hull et al. (10) have shown that a large pulse of Deccan CO<sub>2</sub> release prior to the K/Pg boundary led to only a  $2^{\circ}\text{C}$  warming (10). More precise quantification is difficult because of the uncertain pace and magnitude of Deccan volcanism. Previous work (26) highlighted the short residence time of SO<sub>2</sub> in the stratosphere and suggested that the short transient nature (decadal duration) of the eruptions would not have enough long-term effect to force the climate into an extinction state. It has been argued (16) that even the 5% solar reduction scenario is an overestimate of the cooling effect of Deccan volcanism and that a surface temperature cooling of  $4.5^{\circ}\text{C}$  is more likely (half that of the  $9.7^{\circ}\text{C}$  in our 5% solar dimming scenario). The solar dimming scenarios would also affect the hydrological cycle. Modeled effects for 5% solar dimming include a 14% decrease and poleward shift in precipitation (Table 2

**Table 1. List of the K/Pg climate-forcing scenarios used in this study**

Name in legends and text	Short description name	Description of simulation
Control	Maa_Cntrl	Late Maastrichtian climate. Solar luminosity: 1,357.18 W/m <sup>2</sup>
Decoupled experiments		
Scenario 1	Maa_-5%	5% solar dimming (modeling extreme Deccan cooling scenario or very mild asteroid impact scenarios). Solar luminosity: 1,298.32 W/m <sup>2</sup>
Scenario 2	Maa_-10%	10% solar dimming (modeling lower extreme of impact-caused cooling). Solar luminosity: 1,221.46 W/m <sup>2</sup>
Scenario 3	Maa_-15%	15% (modeling moderate extreme of impact-caused cooling). Solar luminosity: 1,153.6 W/m <sup>2</sup>
Scenario 4	Maa_-20%	20% (modeling extreme of impact-caused cooling). Solar luminosity: 1,085.74 W/m <sup>2</sup>
Scenario 5	Maa_4xCO <sub>2</sub>	×4CO <sub>2</sub> (modeling 1,120-ppm CO <sub>2</sub> injections caused by Deccan volcanism)
Scenario 6	Maa_6xCO <sub>2</sub>	×6CO <sub>2</sub> (modeling 1,680-ppm CO <sub>2</sub> injections caused by Deccan volcanism)
Coupled experiments (transient)		
Scenario 11	Aero100x_+Ash	Aerosol + ash, during impact, ×100 Pinatubo
Scenario 12	Post_Aero100x_+Ash	Aerosol + ash, postimpact, ×100 Pinatubo
Scenario 13	Aero100x_+4CO <sub>2</sub> _+Ash	Aerosol + ash + Deccan, during impact ×100 Pinatubo
Scenario 14	Post_Aero100x_+4CO <sub>2</sub> _+Ash	Aerosol + ash + Deccan, postimpact ×100 Pinatubo

The complete list is in *SI Appendix, Table S1*. A full description of all forcing is in *SI Appendix*.

and *SI Appendix, Figs. S1–S3*), whereas the most extreme (20%) asteroid-induced solar dimming scenario causes a 95% precipitation decrease.

Transient aerosol experiments (Tables 1 and 3) at the K/Pg event, with and without ash deposition (scenarios 11 to 14), show a stark cooling (over the 6-y period where stratospheric aerosols are simulated) in global mean temperature (>34 °C), followed by a recovery to “normal” preboundary conditions (Fig. 2 *G–I*, Table 3, and *SI Appendix, Fig. S7*) over a time frame of decades. Here, two different transient aerosol-forcing experiments were conducted: 1) the K/Pg impact event based on inferred climate forcing as a result of aerosol release and land surface perturbation (18, 20–25) (Table 3) (with a sensitivity study in which this forcing was reduced by half) (*SI Appendix, Table S3*) and 2) a set of simulations whereby release of CO<sub>2</sub> from Deccan volcanism was included (*SI Appendix, Table S3*). These simulate aerosol loading from the asteroid impact (altering optical depth) as well as increased CO<sub>2</sub> from sustained long-term volcanism, both with simulated volcanogenic aerosol effect (scenarios 9 to 14) (Fig. 2 *F*

and *G* and Table 1) and without the latter volcanism-related effects (scenarios 7 and 8) (Fig. 2 *H* and *I* and Table 1). *Materials and Methods* has further details (*SI Appendix*). These simulations reproduce an impact that would have generated the same effect as 100 Pinatubo eruptions, hypothesized to be the same impact on climate as the Chicxulub impactor (29). The Pinatubo eruption in 1991 led to the injection of 18 to 19 Tg of SO<sub>2</sub> into the lower stratosphere, with a 60-fold increase above nonvolcanic levels. The concentrations of SO<sub>2</sub> were still 10× above normal preimpact values after 2-y equilibration time (e-folding) of one (29). This led to planetary cooling of ~0.5 K and took 7 y for SO<sub>2</sub> to return to preeruption levels (29, 30).

After the initial postimpact disturbance of the Cretaceous climate (peak land surface cooling to –34.7 °C globally within 5 y) (*SI Appendix, Fig. S7*), our transient experiments (*SI Appendix, Table S3*) indicate that the climate system recovery would have taken around 30 y; however, this would have been accelerated by ~10 y with the inclusion of volcanically derived increased CO<sub>2</sub> (*SI Appendix, Fig. S7*). In this case, the CO<sub>2</sub> would have enabled the climate to recover to 0 °C ± 5 °C within 10 y of the impact and to preimpact conditions after ~20 y. An ash layer over North America would have further offset ~4 °C to 5 °C of land surface cooling, with a small enhancement in recovery to preimpact temperatures (*SI Appendix, Fig. S7*). The hydrological cycle over land would have been significantly modified, with precipitation reduced by over 85% (Table 3 and *SI Appendix, Figs. S1–S3*) in months after the impact.

Preimpact end-Cretaceous climate data were used to identify the abiotic conditions favorable for non-avian dinosaurs (Fig. 3*A* and *Materials and Methods*). This was used as a baseline from which to evaluate the effect of the various modeled climate perturbations [incorporating the relative uncertainties to a suite of modeled climatic scenarios combined with Ensemble modeling (31) on the potential global distribution of non-avian dinosaur habitat] (Fig. 3*A*). The 5% solar dimming experiment (Fig. 3*B*) leads to a disappearance in peak habitability from pre-K/Pg values, with potential habitat reduced to 4 and 24% in lower habitat suitability thresholds (0.5 and 0.3, respectively) (Fig. 4). At 10% solar dimming, potential habitat is effectively removed (0.4% of pre-K/Pg values) (Fig. 3*C*) at the lowest habitability threshold (0.3) (Fig. 4). Habitat suitability in solar dimming scenarios is completely extinguished at ≥15% dimming. Global habitability increases in models simulating long-term CO<sub>2</sub> injection due to Deccan volcanism, in case an asteroid impact would not have happened (Fig. 3*D* and *E*): maximum dinosaur habitat suitability increases by ~120% at 1,120 ppm of CO<sub>2</sub> and ~97% at 1,680 ppm of CO<sub>2</sub>. These results suggest that long-term Deccan volcanism alone cannot be responsible for complete dinosaur habitat disruption, without invoking unrealistic volcanic SO<sub>2</sub> forcing (near-constant large ejections) not seen at any point in the Phanerozoic (16). Habitat suitability modeling (HSM) shows that regions of lower climatic suitability would still be present in more tropical latitudes for dinosaurs in the 5% and to a lesser degree, in the 10% solar dimming scenarios [forcing too strong according to Schmidt et al. (16)] (Fig. 3). Habitat suitability reaches a critical threshold between the 10 and 15% solar dimming simulations, with no remaining habitat for non-avian dinosaurs in models with 15% dimming (scenarios 3, 4, 7, and 8) (Table 1). Chemical processes are not simulated in these experiments and could further lead to habitat loss.

The transient asteroid experiments show an extinction-level event of the non-avian dinosaurs' climatic niche (Fig. 3*F* and *H*), coincident with the lowest temperatures reached in experimental simulations after asteroid-induced cooling (*SI Appendix, Fig. S3*). Habitat suitability for these taxa (*SI Appendix, Table S4*) then reestablishes differentially in the models with and without long-term Deccan volcanism CO<sub>2</sub> increase. In scenarios simulating active volcanism (CO<sub>2</sub> increase), at the same time as the

**Table 2. K/Pg climate-forcing scenarios**

Experiment	Ocean temperature		SAT			Precipitation		
	SST	666-m Depth	Ocean	Land	Global	Ocean	Land	Global
Control	22.64	12.41	21.65	11.49	18.96	3.5	2.38	3.2
-5% Sol. (Sc 1)	16.93	12.06	14.87	1.83	11.42	3	2.05	2.75
-10% Sol. (Sc 2)	11.06	11.72	4.56	-12.18	0.13	2.5	1.59	2.26
2 × CO <sub>2</sub> > 4 × CO <sub>2</sub> (Sc 5)	25.11	12.56	24.47	16.2	22.28	3.58	2.49	3.29
2 × CO <sub>2</sub> > 6 × CO <sub>2</sub> (Sc 6)	27.02	12.66	26.86	20.24	25.11	3.59	2.5	3.3

The end-Cretaceous climate of the Maastrichtian (control) and perturbations to the mean climate state resulting from a set of solar luminosity (Sol.; watts per meter<sup>2</sup>) reduction experiments at -5 and -10% (additional experiments are presented in *SI Appendix*) and two different scenarios (Sc) of CO<sub>2</sub> injection due to Deccan volcanism. Data are shown for sea surface temperatures (SSTs; degrees Celsius) at intermediate (666-m) ocean water column depth; global, land, and ocean surface air temperatures (SATs; degrees Celsius); and global, land, and ocean precipitation (millimeters per day) for the mean of the last 50 y of each simulation (expanded methods are in *SI Appendix*).

impact, maximum habitability increases 152% from preimpact levels after recovery (Figs. 3 *E* and *G* and 4). In the transient experiments with inactive (no CO<sub>2</sub> release) Deccan volcanism, habitat suitability reaches lower levels than the preimpact scenario, with 135% more end-Cretaceous peak habitability after the ecosystem recovers from the impact (~30 y after). It is likely that in both scenarios this would return to preimpact levels after the climate has fully reequilibrated. In all transient asteroid impact model experiments for HSM (Table 3), the addition of Deccan-sourced CO<sub>2</sub> (scenarios 13 and 14) (Table 1) shows that the short-term transient cooling response is not significantly offset and that eradication of non-avian dinosaur abiotic niche is pronounced (Figs. 3 and 4). On the other hand, recovery rates are accelerated, and postextinction habitability is reestablished at a relatively higher level when coincident volcanism is modeled during the postimpact scenario.

An independent run using MaxEnt (32, 33) was performed to test whether these results would corroborate the outcome from the Ensemble simulations (*Materials and Methods* and *SI Appendix*). The 5% solar dimming experiment leads to a substantial, but noncatastrophic, 50% reduction in peak habitability from pre-K/Pg values (*SI Appendix*, Fig. S18 *A* and *B*). With 10% solar dimming, potential habitat is reduced to 4% of pre-K/Pg values (*SI Appendix*, Fig. S18 *C*) and extinguished at ≥15% dimming. Global habitability is higher in models simulating constant CO<sub>2</sub> injection due to Deccan volcanism (*SI Appendix*, Fig. S18 *D* and *E*): maximum dinosaur habitat suitability increases by ~27% at

1,120 ppm of CO<sub>2</sub> and ~32% at 1,680 ppm of CO<sub>2</sub>, confirming the previous Ensemble results in which long-term Deccan volcanism alone cannot be found responsible for complete dinosaur climatic niche extirpation. The simulated transient asteroid impact experiments (*SI Appendix*, Fig. S18 *F–H*) confirm the same trends of the Ensemble outputs (Fig. 3 *F* and *H*) in providing an almost complete eradication of dinosaur abiotic niche. Even here, habitat suitability for these taxa (*SI Appendix*, Table S4) reestablishes more quickly and at higher "preextinction levels" when active Deccan volcanism-induced CO<sub>2</sub> injection is simulated as active (122% of preimpact levels after recovery) (*SI Appendix*, Figs. S18 *E* and *G* and S19). Analogously with the Ensemble results, inactive Deccan volcanism fosters a recovery to 92% of end-Cretaceous preimpact habitability.

### Discussion

The view of Deccan volcanism (both short and/or long term) as the main abiotic driver of the K/Pg mass extinction is often justified by referring to volcanism as a historically strong influencer of global climate (11, 12). Most pertinently, extensive volcanism is recognized as the primary cause behind the most severe biotic crisis of all time, the end-Permian mass extinction [251 Ma (34)], and possibly the Triassic/Jurassic mass extinction [201 Ma (15)] too. However, the timing and duration of the end-Permian extinction were quite different from those of the K/Pg event, with some organisms disappearing earlier than others (35) over the course of ~10 My. The ocean also acidified and became

**Table 3. Transient aerosol K/Pg extinction simulations**

Experiment	SST		666-m Depth		SAT					Precipitation						
					Ocean		Land		Global		Ocean		Land		Global	
	Before impact	Impact	Before impact	Impact	Before impact	Impact	Before impact	Impact								
Aerosol 100 with ash deposit (Sc 11 and Sc 12)	22.1	2.49	11.81	11.88	21.38	-13.44	10.99	-30.21	18.63	-17.87	3.52	0.78	2.4	0.28	3.22	0.65
Aerosol 100 and 2 × CO <sub>2</sub> > 4 × CO <sub>2</sub> with ash deposit (Sc 13 and Sc 14)	23.93	4.05	11.81	11.88	23.59	-8.23	14.95	-25.96	21.31	-12.92	3.59	0.91	2.51	0.33	3.31	0.75

A set of transient simulations with perturbed aerosol atmospheric optical depth, pCO<sub>2</sub> concentrations, and ash layer deposits is performed over a set of 200-y simulations. Their individual global, land, and oceanic impact on specific climate variables (sea surface temperature [SST; degrees Celsius], surface air temperature [SAT; degrees Celsius], precipitation [millimeters per day]) for the 50-y mean preimpact climate state and the mean of the three coolest years resulting from the postasteroid impact. The complete set of experiments with sensitivity tests is presented in *SI Appendix*. Sc, scenario.

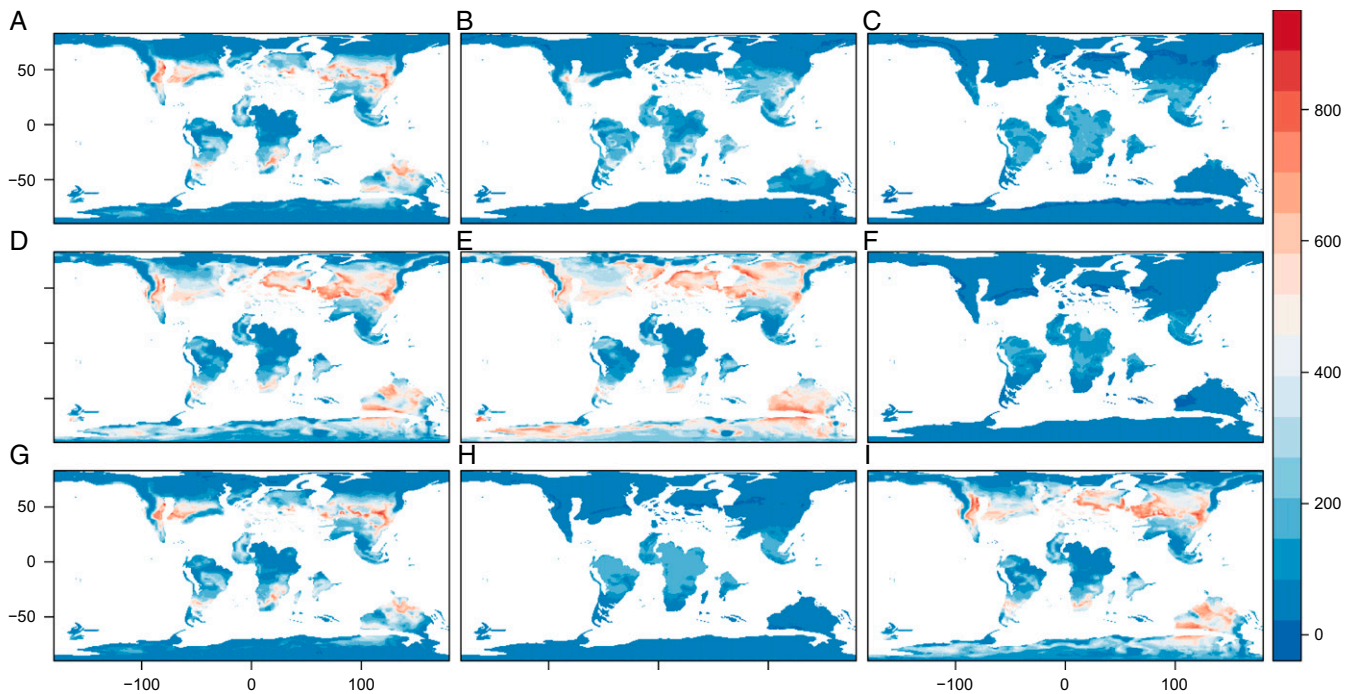


**Fig. 3.** Ensemble habitat suitability models (averaged) projected globally for nine clades of non-avian dinosaurs (additional details and figures on habitat suitability models are in *SI Appendix*). Blue color represents low level of habitat suitability (0), while red color represents high habitability (1,000). Habitat suitability models trained on the late Maastrichtian record and GCMs control (A) are then projected to decoupled solar dimming scenarios with 5% (scenario 1) of solar reduction (B) and (scenario 2) 10% of solar reduction (C). A climatic scenario modeling two different levels of greenhouse enrichment due to the Deccan volcanism is reported in D (scenario 5) and E (scenario 6). The effect on the dinosaur-suitable habitats for two transient simulations with Deccan volcanism inactive (F, scenario 11 and G, scenario 12) and active (H, scenario 13 and I, scenario 14) shows the dynamic response of global dinosaur habitability during the impact (F, scenario 11 and H, scenario 13) and throughout the recovery (G, scenario 12 and I, scenario 14).

anoxic, which is symptomatic of a geologically slow process (36–38). All of this indicates a prolonged and multiphase extinction process (34). Furthermore, a recent study found no correlation between the timing of Deccan volcanism pulses and global climate changes (9, 10), or a large pulse  $10^4$  y prior to the bolide impact, questioning Deccan volcanism’s influence as an abiotic driver of extinction (8). It is noteworthy that even the stratigraphic interbeds of the Deccan Traps have yielded dinosaur and other

terrestrial fossil remains (39, 40) (Fig. 1), indicating that animals were able to survive previous high-intensity eruptions, even within the epicenter of the Deccan region itself. Given India’s geographic isolation at this time, these fossil-bearing beds cannot be explained by biotic restocking via dispersal events (39). Short-term Deccan volcanism (aerosol release), even in the more extreme Deccan-induced 5% solar reduction scenario (with greater sulfur release than hypothesized) (16), does not perturb the mean climate state

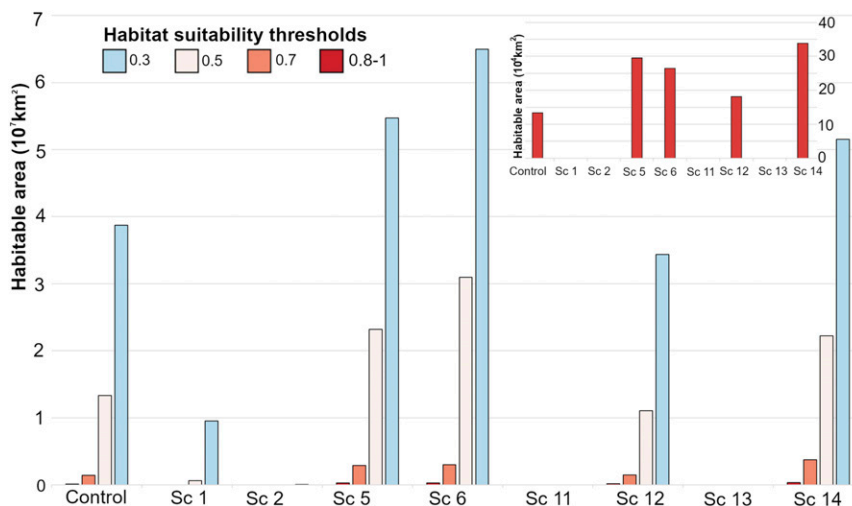


**Fig. 4.** Histogram showing areal amount of habitat suitability for different ensemble HSM averaged in each climatic-forcing scenario (Sc) for all of the clades used. A constant decrease from initial conditions (control) is observed in the solar dimming models (Sc 1, 5% and Sc 2, 10%). A habitability increase is caused by  $4\times\text{CO}_2$  (Sc 5) and  $6\times\text{CO}_2$  (Sc 6) addition. A transient model shows the habitability decrease during the impact-related climatic perturbation and consequent recovery without Deccan volcanism (Sc 11 and 12) and with active volcanism (Sc 13 and 14). (Inset) Maximum thresholds of HSM outputs projected in each Sc.

sufficiently to produce an inhospitable biosphere globally for non-avian dinosaurs. Even assuming the highest intensity of sulfur injections caused by Deccan volcanism (and longest atmospheric residence times), the order of magnitude of these releases barely approaches the lowest estimates of release by the Chicxulub impactor (20–22). Longrich et al. (41) proposed that mammal diversity in latest Cretaceous assemblages [e.g., the North American Hell Creek Formation (42–44)] actually increases following the Deccan eruption. Given that the hypothesized (25) asteroid-induced cooling likely drove the extinction, a pulse of warming (with a similar magnitude as shown in our simulations) (9) just prior to the extinction may have acted as a buffer against cooling induced by the Chicxulub impact, ameliorating the physical effects of bolide impact (41). Such a scenario seems to be supported by the recently described continental record of biotic recovery across the K/Pg boundary (42), in which Lyson et al. (42) presented stratigraphic and paleontological evidence of mammalian increase in diversity and body size, coinciding with warming pulses and radiation of major angiosperm clades and suggesting a possible link with a Deccan-induced greenhouse gasses-enriching effect.

Even within the site of the asteroid impact, rich communities were reestablished within 30 ky of the K/Pg boundary (45). This implies a very rapid recovery of marine productivity (45, 46), which argues against the suggested delay in ecosystem reset caused by continued Deccan volcanism after the K/Pg boundary (9, 45, 46). In contrast to the end-Permian mass extinction, the K/Pg event was geologically instantaneous (2–4, 10, 23, 35), and there is no clear evidence for a prolonged decline (3, 4, 35, 47) that would be required for Deccan volcanism to trigger a mass extinction-level event due to the short residence time of stratospheric aerosols. In addition, studies on marine microfossils from Antarctica are consistent with a sudden, catastrophic driver for the extinction, such as the bolide impact, rather than a significant contribution from Deccan Traps volcanism during the latest Cretaceous (48). Although some authors have argued for a latest Cretaceous decline in dinosaur diversity, other analytical studies are consistent with relatively high preextinction standing diversity, which is compatible with a sudden extinction scenario for non-avian dinosaurs (47). The extinction of only shallow-water marine organisms (12, 45, 48–50) highlights a lack of prolonged deep-water acidification, while conjoined isotopic and Earth System Modeling results show rapid oceanic acidification (49) and subsequent quick recovery (49), compatible with asteroid-induced effects in the ocean. One major implication of such a rapid event for the marine realm is that the extinction driver must have been in play for a duration shorter than the mixing time of ocean waters (~1,000 y) (45, 49). Our simulations (Tables 1 and 2) suggest that sea surface temperatures would have been reduced for all scenarios (*SI Appendix, Figs. S1, S3, S5, and S7*) but that the rest of the water column (>1,000 m) was unaffected (*SI Appendix, Fig. S7B*). After the extinction, the marine environment recovered relatively fast, between a few thousand years to ~1 My (9, 45, 46, 49).

Whether or not Deccan volcanism actively contributed to temperature decline through atmospheric cooling (via SO<sub>2</sub> aerosol release) is still unclear. The emissions resulting from Deccan volcanism also caused a local atmospheric injection of gas and debris (24, 28), reflecting incident solar radiation from the Sun but potentially trapping radiant heat in the lower level of the atmosphere (8, 11, 14). It is even unclear whether the volatile products from the Deccan eruptions reached the stratosphere. With SO<sub>2</sub> stratosphere residence times being of the order of years, pacing of eruptions would have had to be significant, with sustained high-energy activity over tens to hundreds of years (16) to inject a constant supply of climate-cooling aerosols to achieve extinction-driving levels. This rate of volcanism would also have to be at an intensity that would represent a 15 to 20% reduction in solar luminosity range whose climatic impact is shown to be far beyond

that hypothesized (16). Long-term Deccan CO<sub>2</sub> warming would have led to an expansion of dinosaur habitable regions in this study, although the global warming we simulate is slightly higher than suggested by proxy records (~3 °C in scenario 5 as opposed to ~2 °C) (10). A longer-term effect of volcanism would directly [and potentially indirectly through a weakened alkalinity pump (49)] increase CO<sub>2</sub> content, offsetting individual short-term cooling events and increasing habitability.

We show that the abiotic impact of Deccan volcanism was not sufficient to cause the extinction of non-avian dinosaurs, while the effects of the impact alone were enough to cause the extinction. It is more likely that the Deccan's influence after the event might have been of greater importance in determining ecological recovery rates after the asteroid-induced cooling, rather than delaying it (42). This also fits well with a recent recalibration that suggests that much of the heightened volcanic activity occurred after the K/Pg boundary (9, 10).

The lithology of the target rocks collided by the Chicxulub asteroid led to a massive release of hundreds of Gigatonnes (Gt) of sulfates (21, 22, 51), yet it is unknown how much reached the stratosphere (16), with a correlated cooling effect of 27 °C (22). This would have led to 3 to 16 y of subfreezing temperatures and a recovery time of more than 30 y. Results from the most recent IODP (International Ocean Discovery Program) drilling expedition (51) suggest that the estimate of sulfur injected to the atmosphere by the impact should be much higher (325 ± 130 Gt of sulfur and 425 ± 160 Gt of CO<sub>2</sub>), which might have generated cooling for centuries (36). Clearly, the asteroid impact was devastating to Earth's climate, leading to freezing temperatures on land (simulated duration in herein reported experiments of ~30 y), even at the tropics; disrupting large faunal food supply; and destabilizing all trophic levels.

Non-avian dinosaurs were not the only victims of the K/Pg mass extinction. Other vertebrate taxa, such as birds (52, 53), mammals (41, 54), and squamates (55, 56), were affected by severe extinction rates (57), whereas other groups, such as crocodylomorphs, turtles, and choristoderes, were affected to a lesser degree (57–60). Without even accounting for other terrestrial and marine animals affected (or completely wiped out) (1, 61, 62), it appears that organisms from a vast array of different ecologies were hit by the extinction mechanism. An ecological determinant behind the high selectivity of the process may be found in variables like body size, diet, physiology, habitat, and geographic range (5, 57, 63). Many of these ecological traits can be, to a certain degree, linked to temperature fluctuations. We know, for example, that habitat, body size, and geographic ranges in living members of crown group Archosauria are extremely sensitive to thermal excursions (63–65). Ecosystem structure can also be severely affected by drastic temperature variations, with an important impact on biodiversity (66, 67), as it has already been suggested for the K/Pg mass extinction (13). An ecological refugium role, potentially offered by the higher thermal inertia of freshwater environments, microhabitats, or the trophic opportunities provided by the detritus cycle (57, 68), may be a potential explanation behind this differential survivorship process. Refugia from extinction-level temperature excursion might have been found in deep valleys, fluvio-lacustrine systems, coastal regions, and in the tropics, which would have offered shelter for taxa such as birds, mammals, turtles, crocodiles, lizards, and snakes, all of which survived the K/Pg mass extinction with comparatively lower species loss (41, 42, 44, 53, 55). Lowered biotic barriers (69), coinciding with warming pulses (9) that sped up the thermic recovery of the Earth System, might have boosted an ecological recovery and consequent release across the boundary in the earliest Danian (10, 41, 42).

These elements imply a cause–effect relationship between the Chicxulub impactor and the K/Pg mass extinction of non-avian dinosaurs. Furthermore, general circulation models (GCMs) and

HSM simulations suggest that climatically active volcanic by-products might have sped up recovery after an impact winter-induced mass extinction. If this is the case, the perception of Deccan volcanism as a K/Pg extinction driver might need to shift to a paradigm that emphasizes the mitigating effect that volcanism could have had on global cooling and extinction. Our results support the Alvarez hypothesis (23), which attributes the end-Cretaceous mass extinction to a prolonged impact winter, as the most likely explanation for the extinction of non-avian dinosaurs. Although we do not discount the impact from biotic effects or other (not tested here) abiotic drivers (e.g., wildfire, acid rain), these results show that even without them the impact winter would have led to dinosaur demise. We demonstrate the possible climatological threshold necessary to trigger the complete extinction of non-avian dinosaurs. Furthermore, we suggest that Deccan volcanism might have contributed to the survival of many species across the K/Pg boundary and potentially fostered the rapid recovery of life from the most iconic of mass extinctions. This modeling approach has the potential to be used for clades (where sampling is spatially and temporally abundant and robust) to deconvolve the impact of secular climate change as a result of various abiotic forcing.

Although we focus on a more likely terrestrial asteroid impact (18), it has been suggested that a deep ocean impact that does not reach the bathymetric surface could result in a substantial injection of water vapor into the stratosphere. It has been proposed that in such a scenario increased oceanic-derived stratospheric water vapor may have cancelled out any aerosol cooling effect and led to significant surface warming (70). Future studies should focus on investigating the effect of other abiotic drivers (e.g., acidification, halogens, significant surface warming, ultraviolet radiation, fire, carbon cycle disruption) of both asteroid impact and Deccan volcanism, as this may offer another avenue to understand the relative effect of both events.

## Materials and Methods

**GCMs of End-Cretaceous Extinction Scenarios.** The climate simulations were carried out using the coupled AOGCM [HadCM3L-M2.1 (71)]. HadCM3L has contributed to the Coupled Mode Intercomparison Project experiments demonstrating skill at reproducing the modern-day climate (71, 72) and has been used for an array of different paleoclimate experiments (73–75). Unlike previous studies using AOGCMs (18, 76–78) to explore the effect of end-Cretaceous volcanism and asteroid impact (and associated aerosol ejecta), we do not use a modern-day topography and bathymetry, but geologic stage-specific boundary conditions representative of the end-Cretaceous paleogeography instead (6). CO<sub>2</sub> concentrations at the end-Cretaceous were set to 560 ppm, within the range of recent pCO<sub>2</sub> (partial pressure of carbon dioxide) reconstructions (79, 80).

The simulations of the extinction scenarios (*SI Appendix, Table S1*) are separated into their short-term and long-term impact on climate and ultimately, non-avian dinosaur abiotic niche. The simulation of Deccan volcanism scenarios is obtained by perturbing the climate by either sustained stratospheric sulfate aerosol loading or sustained increased CO<sub>2</sub>. Because of uncertainty in the amount of aerosol release from such events, we investigate the impact of volcanism as a function of a constant reduction in solar radiation (solar dimming) at the Earth's surface simulating the radiative cooling effect of sulfate aerosols in the stratosphere. A reduction in solar radiation equal to 5 to 15% has been hypothesized to be comparable for Deccan volcanism (without CO<sub>2</sub> release) (24, 79–81). To test uncertainty of Deccan volcanism stratospheric aerosol loading and associated cooling, we also test the impact of 15 to 20% solar reduction, which can also be used synonymously as an asteroid impact solar luminosity reduction analog due to predicted change in radiative forcing (25).

Sustained volcanic release of CO<sub>2</sub> has been hypothesized (81–84) as a potential mechanism of extinction in the end Cretaceous. Two idealized large injections of CO<sub>2</sub> have been simulated over a 200-y period. Both represent extremes scenarios supported by geological evidence of an increase in CO<sub>2</sub> from the 560-ppm baseline CO<sub>2</sub> in the model to 1) 1,120 ppm (26) and 2) 1,680 ppm (16, 27) CO<sub>2</sub>. Previous attempts in constraining the total volume of eruptive material and volatiles (26) refer to a CO<sub>2</sub> release of 2.1 to 4 times, so that our  $\times 4\text{CO}_2$  scenario models an extreme Deccan release. Numerical

values for the physical parameters in the decoupled (*SI Appendix, Table S2*), and transient coupled (*SI Appendix, Table S3*) are reported.

We prescribe stratospheric sulfate aerosol concentrations as a function of the impact on atmospheric optical depth to simulate an extraterrestrial asteroid impact. Values of optical depths at 0.55  $\mu\text{m}$  were taken from observations (27) of the 1991 Pinatubo eruption with sulfate aerosol loading of the stratosphere equivalent to 100 times the forcing of the Pinatubo eruption (20, 27) consistent with the estimates of Pierazzo et al. (20). The radiative impact of sulfate aerosols is simulated through absorbing and scattering incoming solar radiation across a spectral range of 0.2 to 10  $\mu\text{m}$  assuming a constant aerosol size distribution (85). A stratospheric residence time of  $\sim 6$  y for the sulfate aerosol was implemented taking into account the longer hypothesized residence time of Pierazzo et al. (20) due to increased atmospheric stratification (21, 22) as a result of concurrent surface cooling and stratospheric warming (70). Stratospheric injection of aerosols into the model was initialized at year 40 into the 200-y simulation. Outside of this 6-y asteroid impact aerosol injection window, no aerosols were released as there is no known baseline aerosol concentration for the Maastrichtian time period to apply. To test the sensitivity of the 100 $\times$  Pinatubo forcing, we also simulate the impact of a less severe asteroid impact with a 50 $\times$  Pinatubo set of simulations. The individual impacts of increased CO<sub>2</sub>, ash layer, and 100 $\times$  and 50 $\times$  Pinatubo aerosol forcing were also simulated. Explanations for all simulations are listed in *SI Appendix, Table S1*.

Episodic eruptions over the last 350 ky of the Cretaceous would have increased the amount of CO<sub>2</sub> in the atmosphere, and so, we also consider a set of simulations with and without the impact of CO<sub>2</sub> degassing as a result of Deccan volcanism (*SI Appendix, Table S2*). CO<sub>2</sub> will have the competing effect of increasing global temperature, potentially offsetting the impact of cooling from stratospheric sulfate aerosols. The precise amount of CO<sub>2</sub> released from Deccan volcanism is unknown due to the difficulty in constraining the total volume of eruptive material and volatiles (24). Here, we use a conservative approach by doubling the baseline CO<sub>2</sub> concentration at the start of the simulation. This is greater than predicted for even the most extreme scenarios (24, 86). Although the amount is likely unrealistic, this does evaluate the potential of volcanically derived CO<sub>2</sub> to mitigate for the cooling effects of impact-derived SO<sub>2</sub>.

A set of simulations with and without a continental size ash blanket (87) over North America (latitudes 67.5°N to 15°N and longitudes 26.25°W to 116.25°W) that may have occurred from the fallout is also performed. For simplicity and due to the uncertainty in the longevity of the ash layer, we prescribed the ash layer for the duration of the 200-y simulation. For the composition of the imposed ash layer and soil properties from observations, we follow Jones et al. (87).

A reduction in solar radiation of  $-5$ ,  $-10$ ,  $-15$ , or  $-20\%$  of Maastrichtian solar luminosity is reproduced for increasingly more extreme asteroid impact scenarios (a solar dimming between 10 and 20% has been discussed in published estimates for atmospheric radiative transfer models of sunlight filtration at the K/Pg event) (24, 25). These are obtained by reducing solar luminosity by 5, 10, 15, and 20% for a 200-y period under  $\times 2\text{CO}_2$  conditions (*SI Appendix, Table S2*). This allows a range of hypothesized impact events simulating the effect of different potential magnitudes.

*SI Appendix* has expanded discussion and figures on baseline boundary conditions and simulation of the different extinction scenarios.

**Dinosaur Occurrence Dataset.** The fossil-occurrence dataset was assembled by downloading a comprehensive database of late Maastrichtian (69 to 66 Ma) global dinosaur fossil occurrences from the Paleobiology Database (<https://paleobiodb.org/#/>) on 6 April 2018 (*SI Appendix, Data S1* and *Data S2*), which have been checked for accuracy and cleaned to obtain a dataset of 2,088 entries. These occurrences belong to nine clades of the end-Cretaceous global dinosaurian fauna (76) and comprise the Ankylosauria, Ceratopsidae, Deinonychosauria, Hadrosauridae, Ornithomimosauria, Oviraptorosauria, Pachycephalosauridae, Sauropoda, and Tyrannosauridae. Expanded discussion on spatial occurrences preparation is reported in *SI Appendix*.

**Habitat Suitability Modeling.** GCM-derived environmental variables were chosen based on broad autecological analogy with their most closely related living organisms [crocodiles + birds (88–90)]. We used Pearson's pairwise correlation test to determine collinearity between variables (*SI Appendix, Fig. S8*), keeping only the predictors showing a Pearson's correlation coefficient below 0.7 to prevent overfitting. The climatic variables used for our HSM were the temperatures of the warmest and coldest annual quartiles and the precipitation of the wettest and driest yearly quarters (*SI Appendix, Figs. S9–S17*). These analyses were run in R version 3.5.1 (R Core Team 2018) with the biomod2 package (91, 92) for Ensemble modeling (31) and using

MaxEnt [maximum entropy algorithm (32, 33)] in the java platform version 3.4.1.

All raw data (environmental variables and occurrence data) and modeling outputs are reported in [SI Appendix, Data S1–S14](#).

Expanded discussion on HSM and figures on additional HSM are presented in [SI Appendix](#), with all settings from Ensemble and MaxEnt modeling reported. The scripts for habitat suitability quantification in areal extent are reported in [SI Appendix, Data S13](#) and [S14](#).

**Data Availability.** All datasets, model outputs, and R scripts are reported in [SI Appendix, Data S1–S14](#) and on Figshare (93–106).

**ACKNOWLEDGMENTS.** We are grateful for the efforts of all those who have generated Maastrichtian dinosaur fossil data as well as those who have

1. D. M. Raup, J. J. Sepkoski Jr., Mass extinctions in the marine fossil record. *Science* **215**, 1501–1503 (1982).
2. D. E. Fastovsky, P. M. Sheehan, The extinction of the dinosaurs in North America. *GSA Today* **15**, 4 (2005).
3. A. A. Chiarenza *et al.*, Ecological niche modelling does not support climatically-driven dinosaur diversity decline before the Cretaceous/Paleogene mass extinction. *Nat. Commun.* **10**, 1091 (2019).
4. P. Schulte *et al.*, The Chicxulub asteroid impact and mass extinction at the Cretaceous-Paleogene boundary. *Science* **327**, 1214–1218 (2010).
5. J. D. Archibald *et al.*, Cretaceous extinctions: Multiple causes. *Science* **328**, 973 (2010).
6. A. Farnsworth *et al.*, Climate sensitivity on geological timescales controlled by nonlinear feedbacks and ocean circulation. *Geophys. Res. Lett.* **46**, 9880–9889 (2019).
7. V. E. Courtillot, P. R. Renne, Sur l'âge des trapps basaltiques. *C. R. Geosci.* **335**, 113–140 (2003).
8. B. Schoene *et al.*, U-Pb constraints on pulsed eruption of the Deccan Traps across the end-Cretaceous mass extinction. *Science* **363**, 862–866 (2019).
9. C. J. Sprain *et al.*, The eruptive tempo of Deccan volcanism in relation to the Cretaceous-Paleogene boundary. *Science* **363**, 866–870 (2019).
10. P. M. Hull *et al.*, On impact and volcanism across the Cretaceous-Paleogene boundary. *Science* **367**, 266–272 (2020).
11. D. L. Royer *et al.*, CO<sub>2</sub> as a primary driver of Phanerozoic climate. *GSA Today* **14**, 4–10 (2004).
12. P. Wilf, K. R. Johnson, B. T. Huber, Correlated terrestrial and marine evidence for global climate changes before mass extinction at the Cretaceous-Paleogene boundary. *Proc. Natl. Acad. Sci. U.S.A.* **100**, 599–604 (2003).
13. J. S. Mitchell, P. D. Roopnarine, K. D. Angielczyk, Late Cretaceous restructuring of terrestrial communities facilitated the end-Cretaceous mass extinction in North America. *Proc. Natl. Acad. Sci. U.S.A.* **109**, 18857–18861 (2012).
14. P. R. Renne *et al.*, Time scales of critical events around the Cretaceous-Paleogene boundary. *Science* **339**, 684–687 (2013).
15. D. P. G. Bond, P. B. Wignall, "Large igneous provinces and mass extinctions: An update" in *Volcanism, Impacts, and Mass Extinctions: Causes and Effects*, G. Keller, A. C. Kerr, Eds. (GSA Special Paper, Geological Society of America, 2014), Vol. 505, pp. 29–55.
16. A. Schmidt *et al.*, Selective environmental stress from sulphur emitted by continental flood basalt eruptions. *Nat. Geosci.* **9**, 77–82 (2016).
17. E. Font *et al.*, Deccan volcanism induced high-stress environment during the Cretaceous-Paleogene transition at Zumaia, Spain: Evidence from magnetic, mineralogical and biostratigraphic records. *Earth Planet. Sci. Lett.* **484**, 53–66 (2018).
18. K. Kaiho *et al.*, Global climate change driven by soot at the K-Pg boundary as the cause of the mass extinction. *Sci. Rep.* **6**, 28427 (2016).
19. J. Vellekoop *et al.*, Rapid short-term cooling following the Chicxulub impact at the Cretaceous-Paleogene boundary. *Proc. Natl. Acad. Sci. U.S.A.* **111**, 7537–7541 (2014).
20. E. Pierazzo, A. N. Hahmann, L. C. Sloan, Chicxulub and climate: Radiative perturbations of impact-produced S-bearing gases. *Astrobiology* **3**, 99–118 (2003).
21. J. Bruggen, G. Feulner, S. Petri, Baby, it's cold outside: Climate model simulations of the effects of the asteroid impact at the end of the Cretaceous. *Geophys. Res. Lett.* **44**, 419–427 (2017).
22. K. O. Pope, K. H. Baines, A. C. Ocampo, B. A. Ivanov, Energy, volatile production, and climatic effects of the Chicxulub Cretaceous/Tertiary impact. *J. Geophys. Res.* **102**, 21645–21664 (1997).
23. L. W. Alvarez, W. Alvarez, F. Asaro, H. V. Michel, Extraterrestrial cause for the cretaceous-tertiary extinction. *Science* **208**, 1095–1108 (1980).
24. A.-L. Chenet *et al.*, Determination of rapid Deccan eruptions across the Cretaceous-Tertiary boundary using paleomagnetic secular variation. 2. Constraints from analysis of eight new sections and synthesis for a 3500-m-thick composite section. *J. Geophys. Res.* **114**, B06103 (2009).
25. K. O. Pope, K. H. Baines, A. C. Ocampo, B. A. Ivanov, Impact winter and the Cretaceous/Tertiary extinctions: Results of a Chicxulub asteroid impact model. *Earth Planet. Sci. Lett.* **128**, 719–725 (1994).
26. T. S. Tobin, C. M. Bitz, D. Archer, Modeling climatic effects of carbon dioxide emissions from Deccan Traps volcanic eruptions around the Cretaceous-Paleogene boundary. *Palaeogeogr. Palaeoclimatol.* **478**, 139–148 (2017).
27. M. Sato, J. E. Hansen, M. P. McCormick, J. B. Pollack, Stratospheric aerosol optical depths, 1850–1990. *J. Geophys. Res. Atmos.* **98**, 22987–22994 (1993).
28. S. Self, M. Widdowson, T. Thordarson, A. E. Jay, Volatile fluxes during flood basalt eruptions and potential effects on the global environment: A Deccan perspective. *Earth Planet. Sci. Lett.* **248**, 518–532 (2006).
29. B. J. Soden, R. T. Wetherald, G. L. Stenchikov, A. Robock, Global cooling after the eruption of Mount Pinatubo: A test of climate feedback by water vapor. *Science* **296**, 727–730 (2002).
30. S. Kremser *et al.*, Stratospheric aerosol—observations, processes, and impact on climate. *Rev. Geophys.* **54**, 278–335 (2016).
31. M. B. Araújo *et al.*, Standards for distribution models in biodiversity assessments. *Sci. Adv.* **5**, eaat4858 (2019).
32. S. J. Phillips *et al.*, Opening the black box: An open-source release of Maxent. *Ecography* **40**, 887–893 (2017).
33. J. Elith *et al.*, A statistical explanation of MaxEnt for ecologists. *Divers. Distrib.* **17**, 43–57 (2011).
34. M. W. Broadley *et al.*, End-Permian extinction amplified by plume-induced release of recycled lithospheric volatiles. *Nat. Geosci.* **11**, 682–687 (2018).
35. S. M. Holland, The stratigraphy of mass extinction and recoveries. *Annu. Rev. Earth Planet. Sci.* **48**, 3.1–3.23 (2020).
36. P. Shulte *et al.*, Response—Cretaceous extinctions. *Science* **328**, 975–976 (2010).
37. P. B. Wignall, Large igneous provinces and mass extinctions. *Earth Sci. Rev.* **53**, 1–33 (2001).
38. R. V. White, A. D. Saunders, Volcanism, impact and mass extinctions: Incredible or credible coincidences? *Lithos* **79**, 299–316 (2005).
39. V. V. Kapur *et al.*, Paleoenvironmental and paleobiogeographical implications of the microfossil assemblage from the Late Cretaceous intertrappean beds of the Manawara area, District Dhar, Madhya Pradesh, Central India. *Hist. Biol.* **31**, 1145–1160 (2018).
40. V. R. Guntupalli, A. S. Prasad, "Vertebrate fauna from the Deccan volcanic province: Response to volcanic activity" in *Volcanism, Impacts, and Mass Extinctions: Causes and Effects*, G. Keller, A. C. Kerr, Eds. (GSA Special Paper, Geological Society of America, 2014), Vol. 505, pp. 193–211.
41. N. R. Longrich, J. Scriberas, M. A. Wills, Severe extinction and rapid recovery of mammals across the Cretaceous-Paleogene boundary, and the effects of rarity on patterns of extinction and recovery. *J. Evol. Biol.* **29**, 1495–1512 (2016).
42. T. R. Lyson *et al.*, Exceptional continental record of biotic recovery after the Cretaceous-Paleogene mass extinction. *Science* **366**, 977–983 (2019).
43. G. P. Wilson, Mammalian faunal dynamics during the last 1.8 million years of the Cretaceous in Garfield County, Montana. *J. Mamm. Evol.* **12**, 53–76 (2005).
44. G. P. Wilson, Mammalian extinction, survival, and recovery dynamics across the Cretaceous-Paleogene boundary in northeastern Montana, USA. *Spec. Pap. Geol. Soc. Am.* **503**, 365–392 (2014).
45. C. M. Lowery *et al.*, Rapid recovery of life at ground zero of the end-Cretaceous mass extinction. *Nature* **558**, 288–291 (2018).
46. B. Schaefer *et al.*, Microbial life in the nascent Chicxulub crater. *Geology* **48**, 328–332 (2020).
47. S. L. Brusatte *et al.*, The extinction of the dinosaurs. *Biol. Rev. Camb. Philos. Soc.* **90**, 628–642 (2015).
48. J. D. Witts *et al.*, Macrofossil evidence for a rapid and severe Cretaceous-Paleogene mass extinction in Antarctica. *Nat. Commun.* **7**, 11738 (2016).
49. M. J. Henehan *et al.*, Rapid ocean acidification and protracted Earth system recovery followed the end-Cretaceous Chicxulub impact. *Proc. Natl. Acad. Sci. U.S.A.* **116**, 22500–22504 (2019).
50. J. Vellekoop *et al.*, Type-Maastrichtian gastropod faunas show rapid ecosystem recovery following the Cretaceous-Paleogene boundary catastrophe. *Palaeontology* **63**, 349–367 (2019).
51. N. Artemieva, J. Morgan, Expedition 364 Science Party, Quantifying the release of climate-active gases by large meteorite impacts with a case study of Chicxulub. *Geophys. Res. Lett.* **44**, 10180–10188 (2017).
52. D. J. Field *et al.*, Early evolution of modern birds structured by global forest collapse at the end-Cretaceous mass extinction. *Curr. Biol.* **28**, 1825–1831.e2 (2018).
53. N. R. Longrich, T. Tokaryk, D. J. Field, Mass extinction of birds at the Cretaceous-Paleogene (K-Pg) boundary. *Proc. Natl. Acad. Sci. U.S.A.* **108**, 15253–15257 (2011).
54. T. J. Halliday, P. Upchurch, A. Goswami, Eutherians experienced elevated evolutionary rates in the immediate aftermath of the Cretaceous-Paleogene mass extinction. *Proc. Biol. Sci.* **283**, 20153026 (2016).

55. T. J. Cleary, R. B. J. Benson, S. E. Evans, P. M. Barrett, Lepidosaurian diversity in the Mesozoic-Paleogene: The potential roles of sampling biases and environmental drivers. *R. Soc. Open Sci.* **5**, 171830 (2018).
56. N. R. Longrich, B. A. Bhullar, J. A. Gauthier, Mass extinction of lizards and snakes at the Cretaceous-Paleogene boundary. *Proc. Natl. Acad. Sci. U.S.A.* **109**, 21396–21401 (2012).
57. P. M. Sheehan, D. E. Fastovsky, Major extinctions of land-dwelling vertebrates at the Cretaceous-Tertiary boundary, Eastern Montana. *Geology* **20**, 556–560 (1992).
58. J. D. Archibald, J. J. Bryant, "Differential Cretaceous-Tertiary extinction of non-marine vertebrates; evidence from northeastern Montana" in *Global Catastrophes in Earth History: An Interdisciplinary Conference on Impacts, Volcanism, and Mass Mortality*, V. L. Sharpton, P. D. Ward, Eds. (GSA Special Paper, Geological Society of America, McLean, VA, 1990), Vol. 247, pp. 549–562.
59. M. J. Benton, Mass extinctions among tetrapods and the quality of the fossil record. *Philos. Trans. R. Soc. Lond. B Biol. Sci.* **325**, 369–385 (1989).
60. L. J. Bryant, Non-dinosaurian lower vertebrates across the Cretaceous-Tertiary boundary in northeastern Montana. *Univ. Calif. Publ. Geol. Sci.* **134**, 1–107 (1989).
61. J. Sepkoski, "A compendium of fossil marine animal Genera" in *Bulletins of American Paleontology*, D. Jablonski, M. Foote, Eds. (Paleontological Research Institution, Ithaca, NY, 2002), Vol. 363.
62. R. B. J. Benson, R. J. Butler, Uncovering the diversification history of marine tetrapods: Ecology influences the effect of geological sampling biases. *Geol. Soc. Lond. Spec. Publ.* **358**, 191–208 (2011).
63. F. J. Mazzotti *et al.*, Large reptiles and cold temperatures: Do extreme cold spells set distributional limits for tropical reptiles in Florida? *Ecosphere* **7**, e01439 (2016).
64. G. C. Grigg *et al.*, Thermal relations of very large crocodiles, *Crocodylus porosus*, free-ranging in a naturalistic situation. *Proc. Biol. Sci.* **265**, 1793–1799 (1998).
65. S. C. Andrew *et al.*, Clinal variation in avian body size is better explained by summer maximum temperatures during development than by cold winter temperatures. *The Auk* **135**, 206–217 (2018).
66. N. B. Grimm *et al.*, The impacts of climate change on ecosystem structure and function. *Front. Ecol. Environ.* **11**, 474–482 (2013).
67. F. C. Garcia, E. Bestion, R. Warfield, G. Yvon-Durocher, Changes in temperature alter the relationship between biodiversity and ecosystem functioning. *Proc. Natl. Acad. Sci. U.S.A.* **115**, 10989–10994 (2018).
68. M. A. O'Leary *et al.*, The placental mammal ancestor and the post-K-Pg radiation of placentals. *Science* **339**, 662–667 (2013).
69. N. R. Longrich, J. Vinther, R. A. Pyron, D. Pisani, J. A. Gauthier, Biogeography of worm lizards (Amphisbaenia) driven by end-Cretaceous mass extinction. *Proc. Biol. Sci.* **282**, 20143034 (2015).
70. M. Joshi *et al.*, Global warming and ocean stratification: A potential result of large extraterrestrial impacts. *Geophys. Res. Lett.* **44**, 3841–3848 (2017).
71. P. J. Valdes *et al.*, The BRIDGE HadCM3 family of climate models: HadCM3@Bristol v1.0. *Geosci. Model Dev.* **10**, 3715–3743 (2017).
72. M. Collins, S. F. B. Tett, C. Cooper, The internal climate variability of HadCM3, a version of the Hadley Centre coupled model without flux adjustments. *Clim. Dyn.* **17**, 61–81 (2001).
73. D. J. Lunt *et al.*, Palaeogeographic controls on climate and proxy interpretation. *Clim. Past* **12**, 1181–1198 (2016).
74. A. Marzocchi *et al.*, Orbital control on late Miocene climate and the North African monsoon: Insight from an ensemble of sub-precessional simulations. *Clim. Past* **11**, 1271–1295 (2015).
75. A. T. Kennedy, A. Farnsworth, D. J. Lunt, C. H. Lear, P. J. Markwick, Atmospheric and oceanic impacts of Antarctic glaciation across the Eocene-Oligocene transition. *Philos. Trans. A Math. Phys. Eng. Sci.* **373**, 20140419 (2015).
76. D. J. Beerling, A. Fox, D. S. Stevenson, P. J. Valdes, Enhanced chemistry-climate feedbacks in past greenhouse worlds. *Proc. Natl. Acad. Sci. U.S.A.* **108**, 9770–9775 (2011).
77. C. G. Bardeen, R. R. Garcia, O. B. Toon, A. J. Conley, On transient climate change at the Cretaceous-Paleogene boundary due to atmospheric soot injections. *Proc. Natl. Acad. Sci. U.S.A.* **114**, E7415–E7424 (2017).
78. C. Covey, S. L. Thompson, P. R. Weissman, M. C. Maccracken, Global climatic effects of atmospheric dust from an asteroid or comet impact on Earth. *Global Planet. Change* **9**, 263–273 (1994).
79. D. L. Royer, M. Pagani, D. J. Beerling, Geobiological constraints on Earth system sensitivity to CO<sub>2</sub> during the Cretaceous and Cenozoic. *Geobiology* **10**, 298–310 (2012).
80. G. L. Foster, D. L. Royer, D. J. Lunt, Future climate forcing potentially without precedent in the last 420 million years. *Nat. Commun.* **8**, 14845 (2017).
81. S. Bekki *et al.*, The role of microphysical and chemical processes in prolonging the climate forcing of the Toba eruption. *Geophys. Res. Lett.* **23**, 2669–2672 (1996).
82. D. J. Beerling, B. H. Lomax, D. L. Royer, G. R. Upchurch Jr., An atmospheric pCO<sub>2</sub> reconstruction across the Cretaceous-Tertiary boundary from leaf megafossils. *Proc. Natl. Acad. Sci. U.S.A.* **99**, 7836–7840 (2002).
83. J. D. O'Keefe, T. J. Ahrens, Impact production of CO<sub>2</sub> by the Cretaceous/Tertiary extinction bolide and the resultant heating of the Earth. *Nature* **338**, 247–249 (1989).
84. K. J. Hsü *et al.*, Mass mortality and its environmental and evolutionary consequences. *Science* **216**, 249–256 (1982).
85. D. A. Kring, D. D. Durda, Trajectories and distribution of material ejected from the Chicxulub impact crater: Implications for postimpact wildfires. *J. Geophys. Res.* **107**, E8 (2002).
86. M. Mussard *et al.*, Modeling the carbon-sulfate interplays in climate changes related to the emplacement of continental flood basalts. *Spec. Pap. Geol. Soc. Am.* **505**, 339–352 (2014).
87. M. T. Jones, R. S. J. Sparks, P. J. Valdes, The climatic impact of supervolcanic ash blankets. *Clim. Dyn.* **29**, 553–564 (2007).
88. A. Guisan, U. Hofer, Predicting reptile distributions at the mesoscale: Relation to climate and topography. *J. Biogeogr.* **30**, 1233–1243 (2003).
89. A. T. Peterson, Predicting species' geographic distributions based on ecological niche modeling. *Condor* **103**, 599–605 (2001).
90. A. T. Peterson, L. F. Ball, K. P. Cohoon, Predicting distributions of Mexican birds using ecological niche modelling methods. *Ibis* **144**, E27–E32 (2002).
91. W. Thuiller, D. Georges, R. Engler, biomod2: Ensemble platform for species distribution modeling. R Package Version 3.1-64 (2014). <https://cran.r-project.org/web/packages/biomod2/index.html>. Accessed 4 January 2019.
92. W. Thuiller, B. Lafourcade, R. Engler, M. B. Araujo, BIOMOD—a platform for ensemble forecasting of species distributions. *Ecography* **32**, 369–373 (2009).
93. A. A. Chiarenza, Spatially unique occurrences of the 9 clades of non-avian dinosaurs investigated in this study. Figshare. <https://figshare.com/s/f622a1f38f0047838b15>. Deposited 27 February 2020.
94. A. A. Chiarenza, Spatially unique occurrences of the 9 clades of non-avian dinosaurs investigated in this study and formatted for MaxEnt java platform version 3.4.1. Figshare. <https://figshare.com/s/aaafa840c177ceb783ed0>. Deposited 27 February 2020.
95. A. A. Chiarenza, Maastrichtian land area-clipped environmental variables for Habitat Suitability Modelling for control and extinction scenarios. Figshare. <https://figshare.com/s/4e789bb29534a21005ed>. Deposited 27 February 2020.
96. A. A. Chiarenza, R script for Habitat Suitability Modelling in ENSEMBLE using biomod2. Figshare. <https://figshare.com/s/79db53000d0ed4908499>. Deposited 27 February 2020.
97. A. A. Chiarenza, Ensemble results for single clade Habitat Suitability Modelling for each scenario. Figshare. <https://figshare.com/s/ab50a7242e80b8961c9b>. Deposited 27 February 2020.
98. A. A. Chiarenza, Scenarios averaged results for all clades from Ensemble Habitat Suitability Modelling. Figshare. <https://figshare.com/s/c40954456b737d77a97a>. Deposited 27 February 2020.
99. A. A. Chiarenza, Raw Ensemble results for single clade Habitat Suitability Modelling for each scenario. Figshare. <https://figshare.com/s/332ef357ba7d5ec83264>. Deposited 27 February 2020.
100. A. A. Chiarenza, Raw Ensemble output results for all clades from Ensemble Habitat Suitability Modelling. Figshare. <https://figshare.com/s/da9fa1a67a2b1ac68778>. Deposited 27 February 2020.
101. A. A. Chiarenza, Bias file based on fossil collection localities for MaxEnt (java platform version 3.4.1) analysis. Figshare. <https://figshare.com/s/c097c769707ac0e75f38>. Deposited 27 February 2020.
102. A. A. Chiarenza, Bias file based convex hull background selection for MaxEnt (java platform version 3.4.1) analysis. Figshare. <https://figshare.com/s/3664934081b9237914a8>. Deposited 27 February 2020.
103. A. A. Chiarenza, Original MaxEnt outputs for single clade Habitat Suitability Models in MaxEnt (java platform version 3.4.1) analysis. Figshare. <https://figshare.com/s/0d8f842c7c52dfeeeb>. Deposited 27 February 2020.
104. A. A. Chiarenza, Scenarios-averaged MaxEnt outputs from single clade Habitat Suitability Modelling results in MaxEnt (java platform version 3.4.1) analysis. Figshare. <https://figshare.com/s/f09f7c92df0306c8d37f>. Deposited 27 February 2020.
105. A. A. Chiarenza, R script for binary conversion from raw outputs of Habitat Suitability Modelling (updated from version in Chiarenza *et al.* 2019). Figshare. <https://figshare.com/s/43dde2841968a69e9e09>. Deposited 27 February 2020.
106. A. A. Chiarenza, R script for area calculation from binary converted Habitat Suitability Models (updated from version in Chiarenza *et al.* 2019). Figshare. <https://figshare.com/s/474f92fb8c6ca215e1d0>. Deposited 27 February 2020.